Adhesion-Induced Phase Separation in Soft Materials

Minwoo Kang, Abdullah Nasir, and Katharine E. Jensen*
Department of Physics, Williams College, Williamstown MA USA
(Dated: June 10, 2019)

We characterize the adhesion-induced phase separation in polydimethylsiloxane (PDMS) gels that serves as a basis for fully understanding the four-phase contact zone between soft gels and rigid bodies. We quasi-statically indent the substrate with varying Young's moduli, which allows a measurement of un-crosslinked PDMS volumes for different indentation volumes without changing the surface properties of the gel substrate. In order to visualize and quantify the phase separated volume, we develop a novel technique of dyeing the gel substrate itself such that both the overall gel and the solid surface will simultaneously fluoresce under a confocal microscope. Our measurements are consistent with the previously established 4/3-power law scaling of separated fluid PDMS volume with respect to the indentation volume. Our results indicate a length scale associated with this phase separation phenomenon and further emphasize that elastic, capillary and osmotic forces are all relevant in analyzing soft, adhesive contact mechanics of gels.

I. INTRODUCTION

The study of contact mechanics has had many important implications both in and out of the science lab. From furthering our knowledge of cellular biology, to addressing pertinent issues such as the stickiness of a bandage, an in depth understanding of contacts between solid surfaces is pivotal. One of the key ideas that forms the basis of modern contact mechanics is the concept of surface energy, which is a result of the intermolecular forces that exist on the surface of a material. The Johnson-Kendall-Roberts (JKR) theory argues that experiments to do with solid adhesion depend on the interfacial surface energy, W, and elastic modulus of the system, E. [1]

While JKR theory has formed the crux of modern contact mechanics, it does not account for the contributions of solid surface tension. Surface tension, Υ, is the energetic cost per area to create a new surface via any method, including cutting or stretching; in the case of solids, surface tension can have a different value from surface energy. In fact, it has been recently shown that solid surface tension induces additional penalties against deformation in soft materials at microscopic length scales comparable to Υ/E. [2–6] At this critical elastocapillary length scale, the geometry of a contact zone will depend on the balance between solid surface tension, surface energies, and elastic forces. [7–9]

Thus, the inclusion of surface tension in understanding the contact mechanics of soft gels has provided new insight into which forces are dominant at a given length scale. However, this modified model still fails to describe the full picture of the contact zone. Surface stress, which is concerned with the amount of work done per unit area needed to elastically stretch a surface, is ignored. Consider, for example, a silica sphere indenting a gel substrate. A problem arises at the edge of the contact line, where the current theories predict a surface stress of infinite magnitude.[10] Previous research has either neglected or failed to resolve this theoretical concern: even in more recent work that outlines the significance of surface tension, neither the entirety of the contact line nor the importance of surface stress has been explored. [1]

More recently, however, it has been discovered that the gel and its solvent can phase separate near the contact line. [11] The presence of a fluid phase resolves the issue of divergent surface stress since a fluid has no elastic penalty to make a sharp contact. On the other hand, this implies that the contact between the gel and the rigid body must be described as a four phase contact zone and the compressibility of the gel network as well as the surface stress should be accounted for when describing the geometry of contact.

Recent literature has begun to highlight the presence of phase-separated fluid regimes near the contact line, but it is not yet known which variables determine the volume of such phase separation. [12, 13] Previous investigations have focused on the interplay between osmotic and capillary forces, but such theory fails to account for the bulk effects of indentation on the fluid separation volume, nor does it explain what role this process may play in mediating or even facilitating adhesive contact. [14–16] Also, it has not yet been possible to image the deformed gel network and the fluid volume itself. As a result, the current understanding of the four phase contact zone is incomplete; the additional contact lines due to the liquid phase cannot be cannot be determined precisely.

In this article, we provide a comprehensive analysis of the adhesion-induced phase separation in soft polydimethylsiloxane (PDMS) gels that incorporates elastic, capillary and osmotic forces. Experimentally, we have developed a novel method of visualizing and quantifying the phase separated volume using confocal microscopy. We quasi-statically indent the substrate with varying compliance, which allows a measurement of liquid PDMS volumes for different indentation volumes while maintaining the same surface properties. We further extend the analysis by mechanically indenting the substrate with a

* kej2@williams.edu

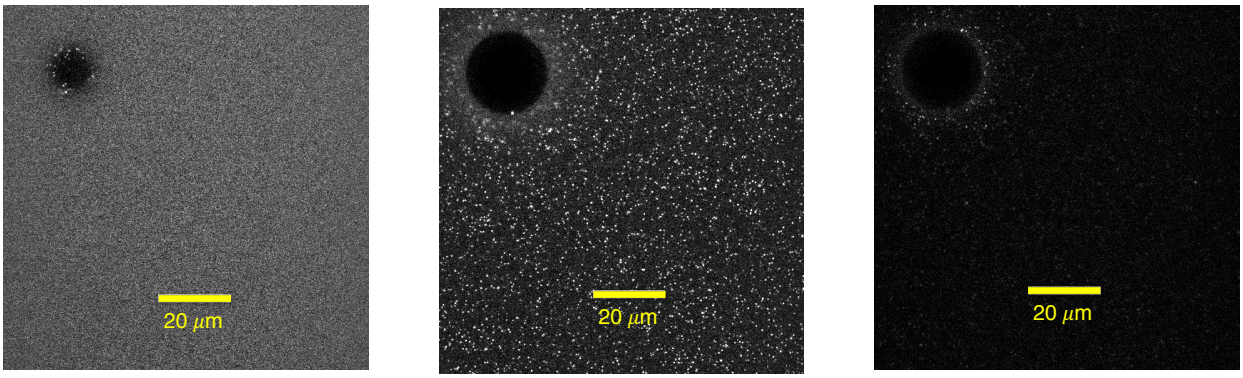

FIG. 1. Raw confocal image slices of a silica sphere in static adhesive contact with a 5 kPa gel substrate. (left to right) Low to high z-axis positions corresponding to $z = -8.6\,\mu$m, $z = 0\,\mu$m and $z = +1.8\,\mu$m.

spherical tip connected to a micro-manipulator

II. EXPERIMENT

We prepare adhesive, compliant silicone gels by mixing liquid PDMS (Gelest DMS-V31) with a chemical crosslinker (Gelest HMS-301) and catalyst (Gelest, SIP6831.2). The first step is to pre-mix a 0.05% weight precent mixture of catalyst in DMS-V31, which we refer to as part A. We also prepare part B, which is a 10% weight precent mixture of crosslinker in liquid PDMS. We then mix parts A and B in appropriate ratios such that the overall weight percent of the catalyst is 0.01%. The mixture is degassed in vacuum, after which a portion is used to spin coat layers of silicone on 0.17-mm thick (# 1.5) microscope cover slips. The remainder is left as a sample for bulk indentation measurements. The resulting substrates are about 120-μm-thick. All silicone samples are cured in air, in an oven at 70°C for at least 24 hours.

We vary the substrate stiffness by adjusting the ratio of polymer to crosslinker. Here, experiments were performed on three levels of Young's moduli, $E = 2.5 \pm 0.1$ kPa, 5.0 ± 0.1 kPa and 10.0 ± 1 kPa. Each value was measured by bulk indentation using a texture analyzer (Texture Technologies, TA.XT Plus). The Poisson ratio of the gel network has been previously measured to be $\nu = 0.48$, [11, 17, 18] and the solvent fractions for each stiffness were 65.2%, 64.7% and 63.7% by weight.

TABLE I. PDMS gel characterization

Mix Ratio (A&B)	Young's Modulus (kPa)	Sol Fraction (%)
11 : 1	2.5 ± 0.1	65.2
9 : 1	5.0 ± 0.1	64.7
7.5 : 1	10.0 ± 1	63.7

In order to observe the fluid phase separation in silicone gel samples, Nile Red Dye is added to the liquid PDMS component **to make 2 to 3% of the total volume of the samples.** After curing, we deposit 40-nm or 100-nm fluorescent beads. We prepare a solution of the fluorescent beads in a buffer solution of sodium tetraborate and boric acid, and apply the solution to the substrate surface for approximately 5 minutes, then rinse them gently with pure water. These beads fluoresce under the blue 488 nm laser so that we can use them as discrete markers to image the surface of the silicone and the subsequent indentation.

Once the samples have been coated with the fluorescent beads, we allow 10-to-50μm-radius silica spheres (Polysciences, 07668) to settle on the substrates. Silica spheres make adhesive contact with the soft gel and thus indent the surface. We allow the spheres to equilibrate for about 20 minutes to 25 minutes. The samples are then imaged using a confocal microscope (Nikon A1R+) in 3D with a 60x water immersion lens. The confocal set up produces slices along the z axis at a step size of 0.225 μm, allowing us to profile the indentation caused by the spheres. Example raw confocal images are shown in Figure 1. The image stack is then imported to a MATLAB-based particle locating software which returns the (x, y, z) coordinates of all fluorescent beads [19, 20]. The data is zeroed and radially (azimuthally) collapsed to yield the (r, z) coordinates.

For comparison against confocal image data, we also prepare silicone substrates appropriate for bright-field microscopy by applying uncured silicone on the edges of standard microscope slides. This process is noted in some of our earlier work [5, 21]. Once cured in the oven, samples have a layer of PDMS that is about 300-μm-thick and a very slight curvature (radius of curvature 700 mum). We then bring the same silica spheres to static, adhesive contact onto the substrate. The sample is illuminated in bright-field under an inverted optical microscope (Nikon Ti2 Eclipse) with a 40x (N.A. = 0.60) objective lens. An example bright-field image of a sphere is shown in Figure 2(b).

III. RESULTS

Nanometer-scale fluorescent beads sit close to the surface of the gel substrate and stay with the solid surface even when the substrate is indented by a rigid sphere.[11] The fluorescent beads, therefore, indicate the position of the solid gel surface, and we map the deformation profile using data from the z-axis confocal image stacks, as shown in Figure 2(a).

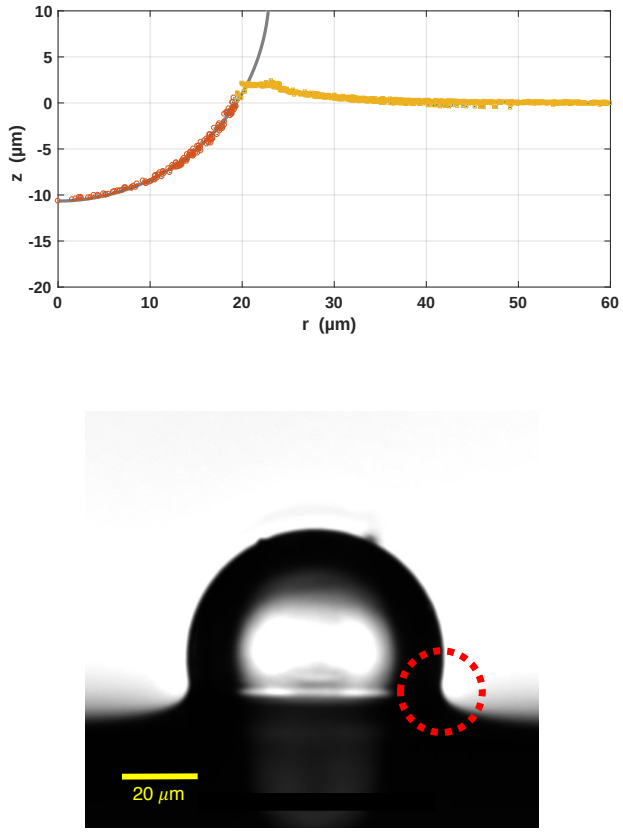

FIG. 2. Surface profiles from confocal and bright-field microscopy. (a) Radial collapse of the confocal data based on locating using MATLAB. (b) A bright-field image of a sphere on a substrate with same stiffness.

As a preliminary step, we analyze the relationship between sphere indentation depth and sphere radius, as shown in Figure 3. Data from the three-level stiffness series of PDMS substrates exhibit an overall slope of 0.85 in the log-log scale. Such slope value implies that the gels we prepared are in the elastocapillary transition regime and so we must consider both elastic and capillary forces when characterizing the force balance in the contact zone.

We also compare the radial collapse profile from confocal images against a sample image from bright-field microscopy shown in Figure 2(b). Notice that the bright-field image shows a sharp, continuous contact line, whereas the solid gel profile indicates a flat cut-off near the fitted circle. The missing fraction of the contact zone corresponds to the regime of uncrosslinked PDMS that has phase separated out from the gel network; the presence of fluid phase allows the gel to satisfy the wetting conditions without introducing infinite surface stress [2, 3, 11].

To answer the question of what determines the volume of fluid phase separation, we plot fluid PDMS volume versus indentation volume. The first method to quantify the fluid volume is to estimate based on the radial collapse data. Since liquid PDMS is incompressible, we can estimate with numerical integration that the volume of phase separated liquid is approximately equal to the difference between the volume that has been indented below the surface and the volume that has been pushed above the original, flat surface[11]. Figure 2(a) indicates these two regimes. The resulting plot is Figure 4: the yellow dots indicate the stiffest substrate ($E = 10$ kPa) substrate, blue the intermediate ($E = 5$ kPa), and red the most compliant ($E = 2.5$ kPa).

Figure 4 shows that for softer substrates, the fluid volume scales by approximately a 4/3-power law with respect to the indentation volume. This result agrees with the scaling law reported in previous literature. [11]. However, the data points obtained from stiffer substrates and smaller silica sphere radii are shown to be rather noisy. In these cases, the fluid volume is very small in terms of magnitude and the numerical volume integration method

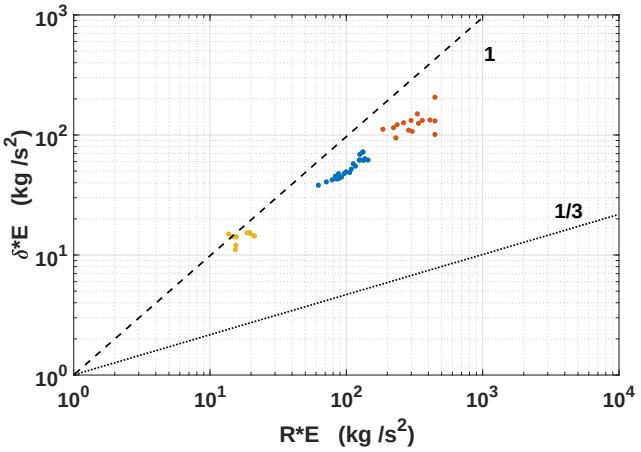

FIG. 3. Plot of indentation depth(δ) $\times$ Young's modulus (E) versus sphere radius (R) $\times$ Young's modulus (E). The dotted line has a slope of 1/3 (elasticity-dominated) and the dashed line has a slope of 1 (capillarity-dominated). Color of data points correspond to varying Young's moduli of the substrates: red, $E = 2.5$ kPa; blue, $E = 5$ kPa; yellow, $E =$ 10kPa. Overall slope of the data points indicate that the gels used in experiments are in the transition regime where both elastic and capillary forces are relevant.

is unreliable. To analyze adhesion-induced phase separation in a more general way, we must take a different approach to measure the fluid volume.

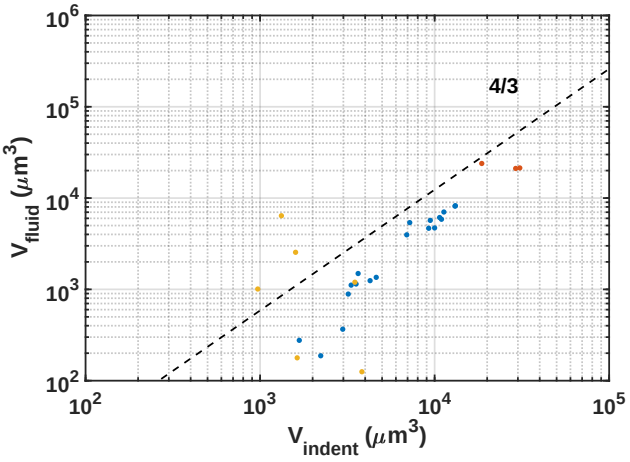

FIG. 4. A log-log plot of fluid volume verses indentation volume for varying Young's moduli. Again, the color of datapoints correspond to varying stiffness of the substrates: red, $E = 2.5$ kPa; blue, $E = 5$ kPa; yellow, $E = 10$kPa. The yellow points, corresponding to measurements from the stiffest substrates, show that the integration method has approached the noise floor.

The alternative technique we developed is to use dyed gel substrates and directly image the entire gel and the solid gel surface simultaneously. An example of a side-slice view of confocal image stacks from a Nile Red dyed sample is shown in Figure 5. With dyed substrates, we can visualize the entire gel including the phase separated fluid volume. This is because the uncrosslinked PDMS also contains the dye and fluoresces with 488-nm light. Simultaneously, the nanometer-scale fluorescent beads mark the solid surface as before. Combining both, we can directly measure volume of separated fluid.

We map the solid surface profile (in red) and the overall gel profile (in blue) on the same plot as in Figure 6 for a preliminary data set. Further refinement of the azimuthal collapse algorithm is required to bring the surfaces to register with each other. This includes finding methods to accurately zero the background gel profile and to better average the pixel intensity values throughout the azimuthal collapse. The separated fluid volume will be represented by a small fraction of blue data points above the flat cutoff of red dots at the contact line.

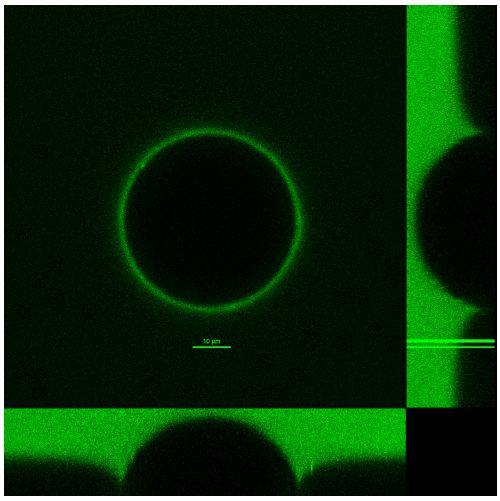

FIG. 5. A side-slice view of the Nile Red dyed sample. Fluorescence of the dye indicates that the gel does make a sharp contact with the silica sphere.

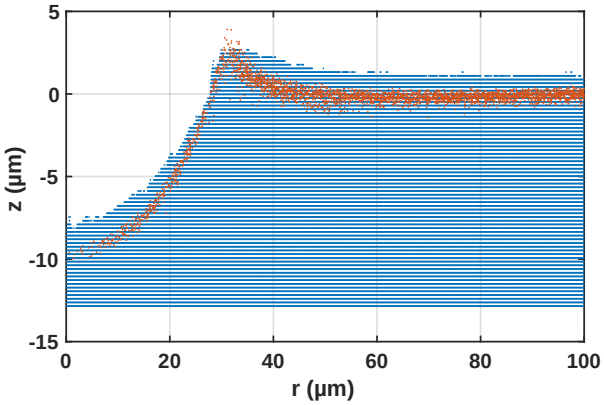

FIG. 6. A rough, preliminary radial collapse plot of both background Nile Red fluorescence and fluorescent nano-bead locating data. Points in blue represent the background, overall fluorescence; red indicate the locations of nm-sized fluorescent beads on the solid surface. In the future, we will calibrate the overlay and improve filtering for background data, so that we can directly measure the phase-separated fluid volume.

IV. DISCUSSION

Many questions remain which we plan to address in the next stage of this study. We first look forward to carrying out the mechanical indentation experiments which will allow us to observe the changes in the separated fluid volume for a wider range of indentation volumes. Hopefully, we will be able to confirm the previously reported 4/3-power law scaling.

However, we also notice that a power-law relation-

ship between separated fluid volume and indentation volume suggests that there exists an associated length scale. What is the physical implication of this quantity? How will this length scale differ from the elasto-capillary length scale, Υ/E?

So far, we have seen that our PDMS gels with Young's modulus $\leq$ 10kPa fall in the transition regime where the gel exhibits both elastic and capillary behavior. But furthermore, since phase separation involves liquid PDMS migrating through and out of the solid gel network, we suspect that the relative viscous flow, or poroelasticity, must be relevant as well [22]. We expect the flow of liquid PDMS to be governed by Darcy's law and will also be determined by the osmotic pressure gradient within the gel. Future work will involve investigating how poroelasticity and the solvent fraction of the gel sets a limit on how much fluid can phase separate out from the gel. In the end, we hope to elucidate what length scale, perhaps a combination of elastic, capillary and osmotic forces, arises in adhesion-induced phase separation.

Furthermore, directly imaging the phase-separated fluid volume will alow us to fully visualize the contact zone. That is, we can finally measure all three contact angles that the fluid volume makes with the rigid sphere, gel substrate and the air [11]. This not implies that there is a non-zero surface tension between the un-crosslinked solvent and the solid gel, but also means that we can finally obtain a full description of the four-phase contact zones exhibited by soft, adhesive gels.

V. CONCLUSIONS AND OUTLOOK

We have seen that a considerable amount of fluid can phase separate at the contact line when sufficiently compliant gels make adhesive contact with rigid spheres. The presence of un-crosslinked PDMS outside the gel network is also expected to have important implications for rough surface adhesion. Future research may consider how the specific geometry might affect the separated fluid volume and thus the adhesive force between the gel substrate and the rough surface. Perhaps one can even think about how to engineer gel properties to either maximize or minimize adhesion. We expect adhesion-induced phase separation to have various implications for industrial and scientific applications, including the design and analysis of pressure-sensitive adhesives (PSAs).

Possible future research also include looking into the cases of heterogeneous gels, such as hydro-gels. Will there be any adhesion-induced phase separation in ionic gels? Can we expand our improved understanding of soft contact mechanics to all types of gels?

[1] K. Johnson, K. Kendall, and A. Roberts, Proc R Soc Lond A Math Phys Sci **324**, 301 (1971).

[2] R. W. Style, C. Hyland, R. Boltyanskiy, J. S. Wettlaufer, and E. R. Dufresne, Nat Comm **4**, 2728 (2013).

[3] X. Xu, A. Jagota, and C.-Y. Hui, Soft Matter **10**, 4625 (2014).

[4] C.-Y. Hui, T. Liu, T. Salez, E. Raphael, and A. Jagota, Proc R Soc Lond A Math Phys Sci **471**, 20140727 (2015).

[5] Q. Xu, K. E. Jensen, R. Boltyanskiy, R. Sarfati, R. W. Style, and E. R. Dufresne, Nature Communications **8**, 555 (2017).

[6] Q. Xu, R. W. Style, and E. R. Dufresne, Soft Matter **14**, 916 (2018).

[7] B. Andreotti, O. Bäumchen, F. Boulogne, K. E. Daniels, E. R. Dufresne, H. Perrin, T. Salez, J. H. Snoeijer, and R. W. Style, Soft Matter **12**, 2993 (2016).

[8] R. W. Style, A. Jagota, C.-Y. Hui, and E. R. Dufresne, Annual Review of Condensed Matter Physics **8**, 99 (2017).

[9] J. Bico, E. Reyssat, and B. Roman, Annual Review of Fluid Mechanics **50**, 629 (2018).

[10] D. Maugis, Langmuir **11**, 679 (1995).

[11] K. E. Jensen, R. Sarfati, R. W. Style, R. Boltyanskiy, A. Chakrabarti, M. K. Chaudhury, and E. R. Dufresne, Proceedings of the National Academy of Sciences **112**, 14490 (2015).

[12] J. T. Pham, F. Schellenberger, M. Kappl, and H.-J. Butt, Physical Review Materials **1**, 015602 (2017).

[13] M. Zhao, J. Dervaux, T. Narita, F. Lequeux, L. Limat, and M. Roché, Proceedings of the National Academy of Sciences **115**, 1748 (2018).

[14] Q. Liu and Z. Suo, Extreme Mechanics Letters **7**, 27 (2016).

[15] Y. Hu and Z. Suo, Acta Mechanica Solida Sinica **25**, 441 (2012).

[16] A. Hourlier-Fargette, A. Antkowiak, A. Chateauminois, and S. Neukirch, Soft Matter **13**, 3484 (2017).

[17] M. Ina, Z. Cao, M. Vatankhah-Varnoosfaderani, M. H. Everhart, W. F. Daniel, A. V. Dobrynin, and S. S. Sheiko, ACS Macro Letters **6**, 854 (2017).

[18] R. W. Style, R. Boltyanskiy, G. K. German, C. Hyland, C. W. MacMinn, A. F. Mertz, L. A. Wilen, Y. Xu, and E. R. Dufresne, Soft Matter **10**, 4047 (2014).

[19] Y. Gao and M. L. Kilfoil, Opt Express **17**, 4685 (2009), we use the particle locating software described in this publication, which is available under "MATLAB 3D feature finding algorithms" at http://people.umass.edu/kilfoil/downloads.html.

[20] K. E. Jensen and N. Nakamura, Review of Scientific Instruments **87** (2015), 10.1063/1.4952992.

[21] K. E. Jensen, R. W. Style, Q. Xu, and E. R. Dufresne, Physical Review X **7**, 041031 (2017).

[22] J. D. Berman, M. Randeria, R. W. Style, Q. Xu, J. Nichols, A. Duncan, M. Lowenberg, E. Dufresne, and K. Jensen, Soft Matter (to be published) (2018).